





Cite this: *RSC Adv.*, 2023, 13, 31213

# Triazine diphosphonium tetrachloroferrate ionic liquid immobilized on functionalized halloysite nanotubes as an efficient and reusable catalyst for the synthesis of mono-, bis- and tris-benzothiazoles†

Farzaneh Gholamhossein Zadeh,<sup>a</sup> Beheshteh Asadi,<sup>a</sup> Iraj Mohammadpoor-Baltork, <sup>\*a</sup> Shahram Tangestaninejad, <sup>a</sup> Valiollah Mirkhani,<sup>a</sup> Majid Moghadam <sup>a</sup> and Akbar Omidvar<sup>b</sup>

Aminopropyl-1,3,5-triazine-2,4-diphosphonium tetrachloroferrate immobilized on halloysite nanotubes [(APTDP)(FeCl<sub>4</sub>)<sub>2</sub>@HNT] was prepared and fully characterized using different techniques such as FT-IR, thermogravimetric analysis (TGA), SEM/EDX, elemental mapping, TEM, ICP-OES, and elemental analysis (EA). This nanocatalyst was found to be highly effective for synthesis of various benzothiazole derivatives in excellent yields under solvent-free conditions. Furthermore, bis- and tris-benzothiazoles were smoothly synthesized from dinitrile and trinitrile in the presence of this catalytic system. High yields and purity, easy work up procedure, high catalytic activity (high TON and TOF) and easy recovery and reusability of the catalyst make this method a useful and important addition to the present methodologies for preparation of these vital heterocyclic compounds.

Received 13th August 2023  
Accepted 29th September 2023

DOI: 10.1039/d3ra05491h

rsc.li/rsc-advances

## Introduction

Ionic liquids (ILs) have attracted increasing interest in the last decades, owing to expanded range of applications and potential advantages including tunable polarity, nonflammability, negligible vapor pressure, large liquid range, and wide solubility.<sup>1</sup> Among them, phosphonium-based ILs are remarkable worthy choices for catalysis because of their desirable properties such as high thermal stability, ionic conductivity and electrochemical windows as well as low viscosity.<sup>2</sup> However, the need for relatively large amounts of these catalysts, the difficulty of separation from the reaction mixture and non reusability<sup>1b</sup> can be considered the drawbacks of the ILs which limit their practical applications. These restrictions can be overcome by the heterogenization of homogeneous catalysts on solid supports. In this context, halloysite nanotubes (HNTs) with a molecular formula of Al<sub>2</sub>Si<sub>2</sub>O<sub>5</sub>(OH)<sub>4</sub>·2H<sub>2</sub>O (1:1 ratio of Al/Si) have attracted considerable attention because of their suitable advantages such as large surface area, biocompatibility, ease of reusability, low price, environmental friendliness, high

mechanical and thermal stability, and resistibility against organic solvents.<sup>3</sup>

Therefore, HNTs have emerged as a highly efficient supports in the fields of catalysis,<sup>4</sup> pharmaceutical studies,<sup>5</sup> industry,<sup>6</sup> and food safety.<sup>7</sup>

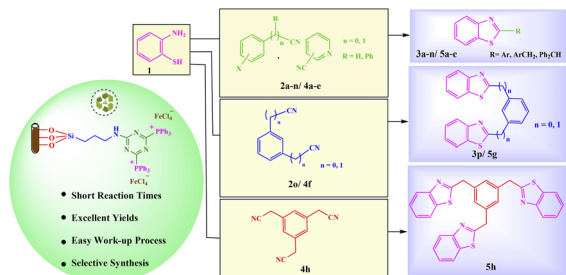
Benzothiazoles are useful building blocks for a number of naturally occurring products<sup>8</sup> and pharmaceuticals with remarkable biological activities such as anticancer,<sup>9</sup> anti-tumor,<sup>10</sup> anti-diabetic,<sup>11</sup> and anti-Alzheimer drugs.<sup>12</sup> Therefore, the development of new methods for the synthesis of benzothiazole derivatives can create a fascinating window in chemistry. For instance, it was reported that benzothiazoles skeletons could be obtained through the condensation of 2-aminothiophenol and aryl/alkyl nitriles using ZnO-nanoparticles as a catalyst.<sup>13</sup> The reaction of 2-aminothiophenol with orthoesters in the presence of catalytic amounts of Bi(III) salts, has been also reported for the synthesis of benzothiazoles under solvent-free conditions.<sup>14</sup> This structure could also be generated from *o*-phenylenediamine and *N*-substituted formamides (C1 sources) via a one-pot protocol catalyzed by zinc in the presence of poly(methylhydrosiloxane).<sup>15</sup> Yu *et al.*, have also reported the Brønsted acid-catalyzed synthetic method for benzothiazoles under metal and solvent-free conditions.<sup>16</sup> Moreover, one-pot syntheses of these heterocyclic compounds has been described through condensation reactions employing Cu(OAc)<sub>2</sub>.<sup>17</sup> However, some of these methods suffer from disadvantages such as acidic or alkaline conditions, high

<sup>a</sup>Department of Chemistry, Catalysis Division, University of Isfahan, Isfahan 81746-73441, Iran. E-mail: imbaltork@sci.ui.ac.ir

<sup>b</sup>Department of Physical Chemistry, Faculty of Chemistry, University of Isfahan, Isfahan, 81746-73441, Iran

† Electronic supplementary information (ESI) available. See DOI: <https://doi.org/10.1039/d3ra05491h>





Scheme 1 Synthesis of mono-, bis- and tris-benzothiazole catalyzed by [(APTDP)(FeCl<sub>4</sub>)<sub>2</sub>]@HNT.

temperature (up to 120 °C) and long reaction times (18 h). Consequently, the development of simple and environmentally benign synthetic methods for the synthesis of such fine heterocycles is of practical importance and still in demand.

Prompted by these results and in continuation of our efforts to develop novel heterogeneous catalytic systems,<sup>18</sup> herein, we wish to report aminopropyl-1,3,5-triazine-2,4-diphosphonium tetrachloroferrate immobilized on halloysite nanotubes as an efficient and easy reusable catalyst for the synthesis of mono-, bis- and tris-benzothiazoles under solvent-free and green conditions (Scheme 1).

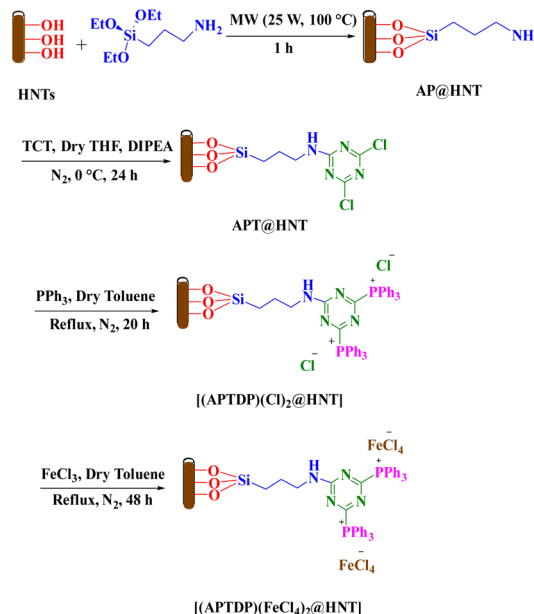
## Results and discussion

### Synthesis and characterization of aminopropyl-1,3,5-triazine-2,4-diphosphonium tetrachloroferrate immobilized on halloysite nanotubes [(APTDP)(FeCl<sub>4</sub>)<sub>2</sub>]@HNT

The synthetic pathway of nanocatalyst [(APTDP)(FeCl<sub>4</sub>)<sub>2</sub>]@HNT is depicted in Scheme 2. First, AP@HNT was synthesized under microwave irradiation according to our previously reported method.<sup>18b</sup> Then, the reaction of 1,3,5-trichlorotriazine (TCT) with the surface-attached aminopropyl of AP@HNT was carried out for substitution of one of the chlorine atoms, to yield APT@HNT<sup>18b</sup> which in turn was converted to [(APTDP)(Cl)<sub>2</sub>]@HNT upon reaction with PPh<sub>3</sub>. Finally, [(APTDP)(Cl)<sub>2</sub>]@HNT reacted with FeCl<sub>3</sub> to produce [(APTDP)(FeCl<sub>4</sub>)<sub>2</sub>]@HNT (Scheme 2).

These processes were monitored by FT-IR, thermogravimetric analysis (TGA), SEM/EDX, elemental mapping, TEM, ICP-OES, and elemental analysis (EA).

The FT-IR spectrum of halloysite nanotubes revealed a number of characteristic peaks at 3694 and 3623, 910, 1034 and 463–537 cm<sup>-1</sup> which can be ascribed to OH groups, Al–OH bending, Si–O stretching and Si–O bending vibrations, respectively (Fig. 1a). The result of this analysis is in agreement with the previous work.<sup>18b</sup> In addition, the presence of bands at 3431 and 3356 cm<sup>-1</sup> (NH<sub>2</sub> stretching vibration), 2933 and 2880 cm<sup>-1</sup> (C–H stretching vibration), and 1654–1581 cm<sup>-1</sup> (NH<sub>2</sub> bending vibration) confirms the synthesis of AP@HNT (Fig. 1b).<sup>18b</sup> As can be seen in Fig. 1c, the FT-IR spectrum of APT@HNT displayed characteristic bands at around 3432 cm<sup>-1</sup> (NH stretching vibration), 1617 cm<sup>-1</sup> (C=N), 1514 cm<sup>-1</sup> (NH bending vibration), 1312 and 1228 cm<sup>-1</sup> (C–N stretching vibration), confirming that the TCT was covalently immobilized onto the



Scheme 2 Synthesis of nanocatalyst [(APTDP)(FeCl<sub>4</sub>)<sub>2</sub>]@HNT.

surface of the nano-clay through formation of C–N bond, but it was not possible to assign the C–Cl band of TCT at 1035–1100 cm<sup>-1</sup>, due to interference of the Si–O stretching band at 1000–1100 cm<sup>-1</sup>. Furthermore, the absorption band at 1469 and 1457 cm<sup>-1</sup> in Fig. 1d and e may approve that the PPh<sub>3</sub> is attached.

Fig. 2 shows the TGA analysis of the [(APTDP)(FeCl<sub>4</sub>)<sub>2</sub>]@HNT sample, which provides information about the thermal stability of this nanocatalyst. As seen in the TGA curve, the initial weight loss (~3.14%) is related to the removal of water molecules within the range of 30–180 °C. the second weight loss (~22.85%) corresponds to the departure of linker and organic

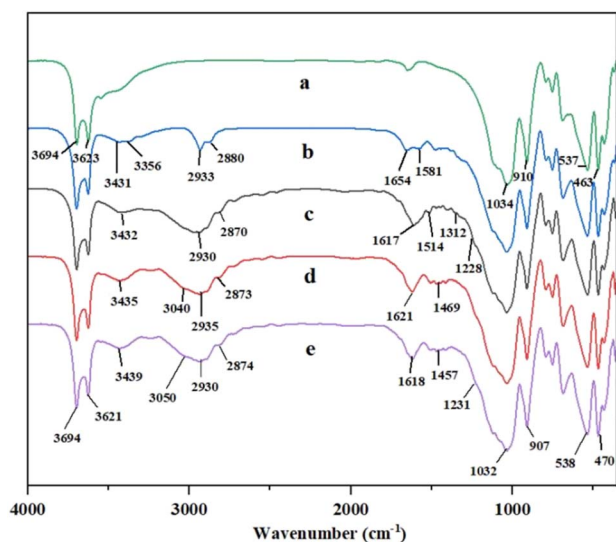


Fig. 1 The FT-IR spectra of: (a) HNT, (b) AP@HNT, (c) APT@HNT, (d) [(APTDP)(Cl)<sub>2</sub>]@HNT and (e) [(APTDP)(FeCl<sub>4</sub>)<sub>2</sub>]@HNT.



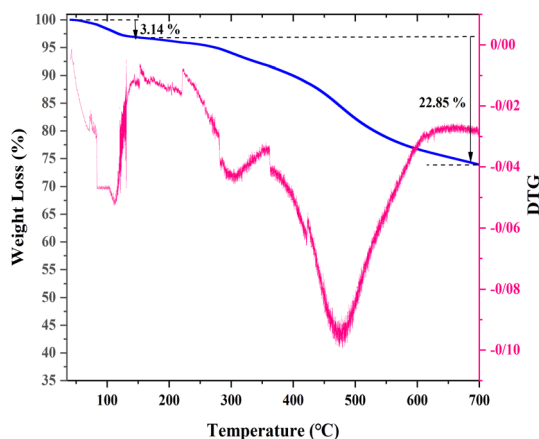


Fig. 2 Thermogravimetric analysis of the [(APTDP)(FeCl<sub>4</sub>)<sub>2</sub>@HNT] nanocatalyst.

moieties, was occurred at around 180–680 °C. Based on these results, the aminopropyl-1,3,5-triazine-2,4-diphosphonium tetrachloroferrate ionic liquid has covalently been linked to nanoclay and can be applied in a wide range of temperatures.

The morphology of the surfaces of HNTs and [(APTDP)(FeCl<sub>4</sub>)<sub>2</sub>@HNT] were examined using scanning electron microscopy (SEM) (Fig. 3a and b). It is noteworthy that the morphology of the two samples is diverse, and also, the geometric shape of the prepared nanoparticles is tubular without aggregation. Furthermore, in order to confirm the presence of Fe and other elements in the final catalyst, the energy dispersive X-ray (EDX) analysis was applied, which obviously illustrated the presence of C, N, P, Cl, O, Al, Si and Fe in catalyst texture (Fig. 3c).

EDX elemental mapping was also indicated that the nanocatalyst was successfully formed owing to the uniform scattering of C, N, P, Cl, O, Al, and Si, and also, the Fe complex was homogeneously dispersed on the functionalized halloysite nanotubes, without any aggregation (Fig. 4). This figure supports the SEM/EDX results (Fig. 3).

To confirm and determine the nanostructure of [(APTDP)(FeCl<sub>4</sub>)<sub>2</sub>@HNT], we performed transmission electron microscopy (TEM) technique (Fig. 5). Based on the results of this analysis, the average particle size of [(APTDP)(FeCl<sub>4</sub>)<sub>2</sub>@HNT] is about 50–80 nm (Fig. 5c) with a well-defined tubular structure.

The FT-IR, TGA, SEM/EDX, elemental mapping, and TEM information show that the [(APTDP)(FeCl<sub>4</sub>)<sub>2</sub>@HNT] catalyst was shaped well by using this process. Besides, the ferric content of the catalyst was measured by ICP analysis and showed a value of 0.60 mmol g<sup>-1</sup> of the [(APTDP)(FeCl<sub>4</sub>)<sub>2</sub>@HNT] of nanocatalyst. This is in good agreement with the values of elemental analysis, which was found to be: C, 11.44; H, 2.69; and N, 1.56. Based on the nitrogen content, the amount of IL immobilized onto the HNT was determined about 0.58 mmol g<sup>-1</sup> of the nanocatalyst.

#### Synthesis of benzothiazole derivatives catalyzed by [(APTDP)(FeCl<sub>4</sub>)<sub>2</sub>@HNT]

We initiated our studies by using 2-aminothiophenol **1** (1.0 mmol) and benzonitrile **2a** (1.0 mmol) as model substrates for



Fig. 3 SEM images of: (a) HNTs, (b) [(APTDP)(FeCl<sub>4</sub>)<sub>2</sub>@HNT], and (c) SEM/EDX spectrum of [(APTDP)(FeCl<sub>4</sub>)<sub>2</sub>@HNT].

optimization of reaction parameters; the results are summarized in Table 1. The model reaction was first performed in the absence of catalyst under solvent-free conditions at 80 °C. No product was obtained under this condition (Table 1, entry 1). In order to achieve the most appropriate conditions, various Lewis





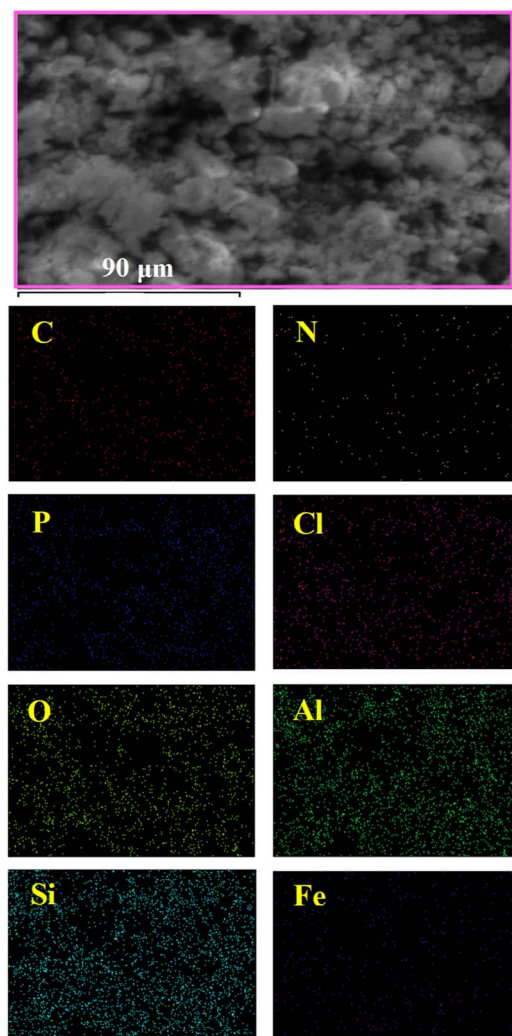


Fig. 4 Energy dispersive X-ray (EDX) mapping analysis of [(APTDP)(FeCl<sub>4</sub>)<sub>2</sub>@HNT].

and Brønsted acids, such as ZnCl<sub>2</sub>, FeCl<sub>3</sub>, InCl<sub>3</sub>, BiCl<sub>3</sub>, ZnO, NaHSO<sub>4</sub>, Fe(HSO<sub>4</sub>)<sub>3</sub>, Al(HSO<sub>4</sub>)<sub>3</sub>, *p*-TSA, NaFeCl<sub>4</sub>, NaFeCl<sub>4</sub>@HNT, HNT, [(APTDP)(Cl)<sub>2</sub>@HNT] and [(APTDP)(FeCl<sub>4</sub>)<sub>2</sub>@HNT] were examined (Table 1, entries 2–15). Amongst them [(APTDP)(FeCl<sub>4</sub>)<sub>2</sub>@HNT] proved to be superior, producing **3a** in 95% yield (Table 1, entry 15). Notably, the activity of [(APTDP)(FeCl<sub>4</sub>)<sub>2</sub>@HNT] can be attributed to the isolation of catalytic active sites on the high surface area of halloysite nanotube. A survey of the amount of [(APTDP)(FeCl<sub>4</sub>)<sub>2</sub>@HNT] revealed that 1.5 mol% is the best choice (Table 1, entry 15), with no improvement upon increasing the catalyst loading to 2 mol% (Table 1, entries 15–17). For temperature optimization (Table 1, entries 18–20), when the reaction was performed at 80 °C, significant improvement was observed with maximum yield of **3a** (Table 1, entry 15). In accordance with Table 1, the optimal reaction conditions were 2-aminothiophenol (1.0 mmol) and benzonitrile (1.0 mmol) in the presence of [(APTDP)(FeCl<sub>4</sub>)<sub>2</sub>@HNT] (1.5 mol%, 25 mg) at 80 °C under solvent-free conditions.

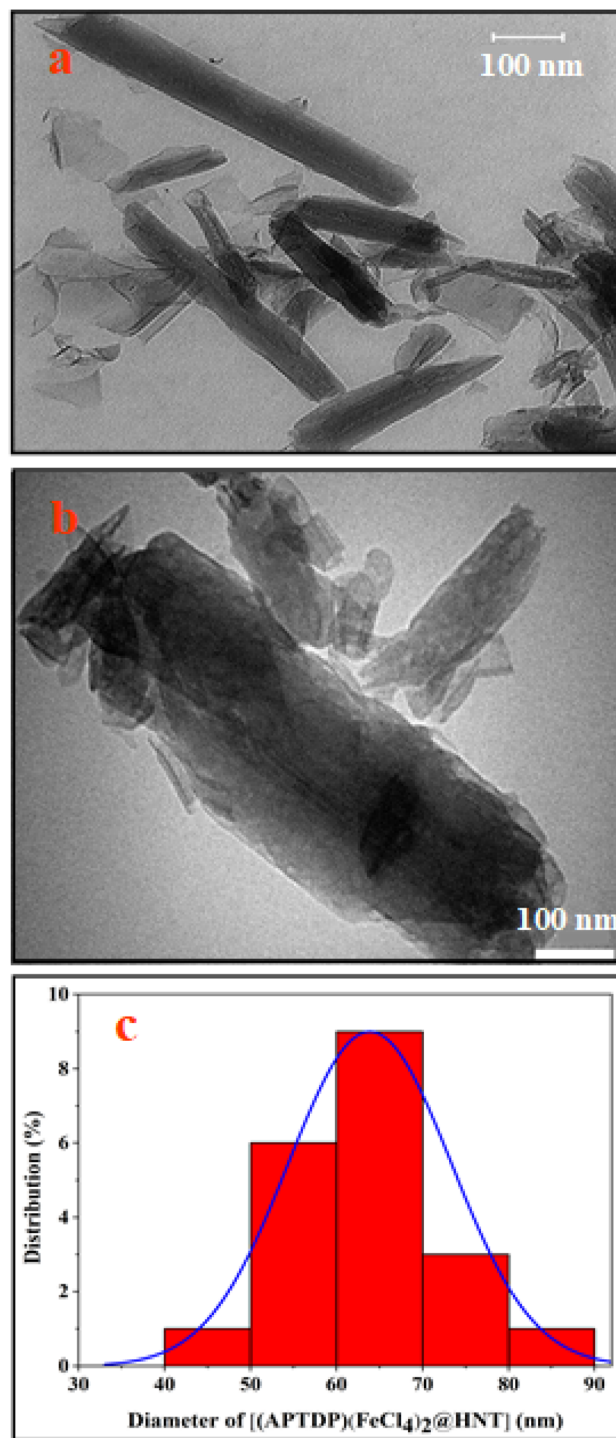


Fig. 5 TEM image of: (a) HNT, (b) [(APTDP)(FeCl<sub>4</sub>)<sub>2</sub>@HNT] and (c) particle size distribution for [(APTDP)(FeCl<sub>4</sub>)<sub>2</sub>@HNT].

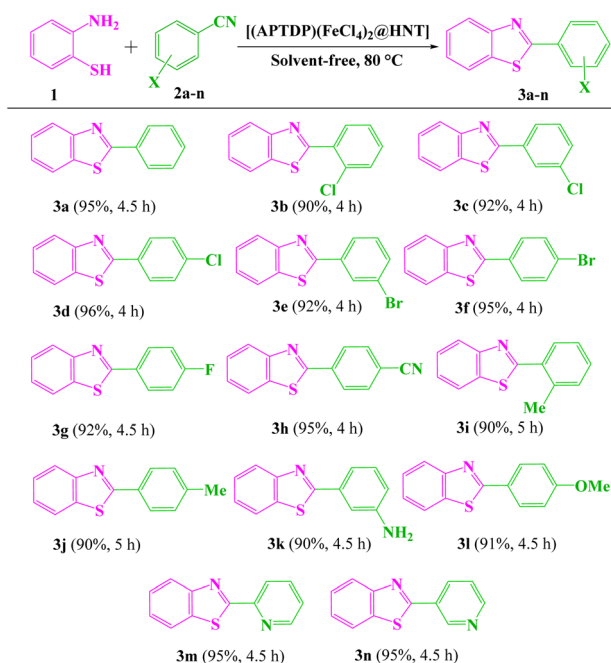
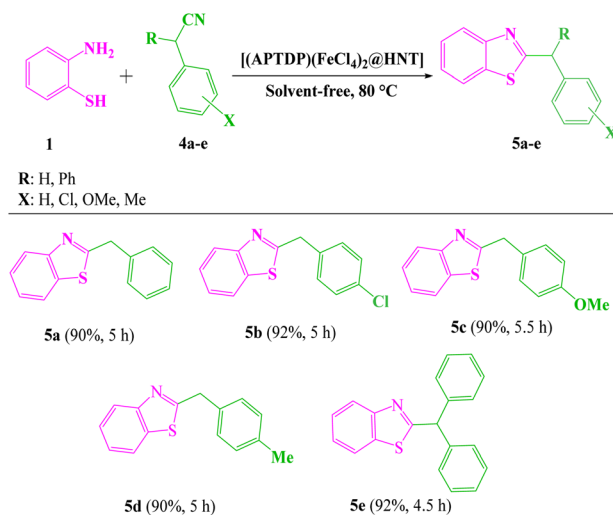
With the optimized experimental conditions in hand, the scope and generality of this methodology was checked by varying the aryl nitrile derivatives (**2a–l**) containing various electron-withdrawing and donating substituents (Scheme 3). The corresponding products **3a–l** were obtained in 90–96% yields within 4–5 h. Significantly, heterocyclic nitriles such as 2- and 3-cyanopyridine yielded the expected products (**3m, n**) in



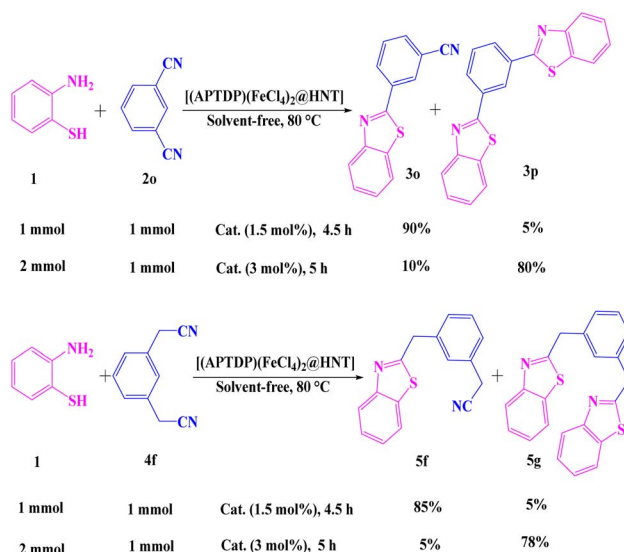
**Table 1** Optimized reaction conditions for the synthesis of benzo-thiazole derivatives<sup>a</sup>

Entry	Catalyst (mol%)	T (°C)	Time (h)	Yield <sup>b</sup> (%)
1	—	80	12	0
2	ZnCl <sub>2</sub> (1.5)	80	4.5	50
3	FeCl <sub>3</sub> (1.5)	80	4.5	50
4	InCl <sub>3</sub> (1.5)	80	4.5	0
5	BiCl <sub>3</sub> (1.5)	80	4.5	5
6	ZnO (1.5)	80	4.5	20
7	NaHSO <sub>4</sub> (1.5)	80	4.5	10
8	Fe(HSO <sub>4</sub> ) <sub>3</sub> (1.5)	80	4.5	20
9	Al(HSO <sub>4</sub> ) <sub>3</sub> (1.5)	80	4.5	20
10	<i>p</i> -TSA (1.5)	80	4.5	35
11	NaFeCl <sub>4</sub> (1.5)	80	4.5	65
12	NaFeCl <sub>4</sub> @HNT (25 mg)	80	4.5	40
13	HNT (25 mg)	80	4.5	0
14	[(APTDP)(Cl) <sub>2</sub> @HNT] (25 mg)	80	4.5	0
15	[(APTDP)(FeCl <sub>4</sub> ) <sub>2</sub> @HNT] (1.5)	80	4.5	95
16	[(APTDP)(FeCl <sub>4</sub> ) <sub>2</sub> @HNT] (0.8)	80	4.5	60
17	[(APTDP)(FeCl <sub>4</sub> ) <sub>2</sub> @HNT] (2)	80	4.5	95
18	[(APTDP)(FeCl <sub>4</sub> ) <sub>2</sub> @HNT] (1.5)	25	4.5	5
19	[(APTDP)(FeCl <sub>4</sub> ) <sub>2</sub> @HNT] (1.5)	50	4.5	45
20	[(APTDP)(FeCl <sub>4</sub> ) <sub>2</sub> @HNT] (1.5)	100	4.5	95

<sup>a</sup> Experimental conditions: 2-aminothiophenol (1.0 mmol), benzonitrile (1.0 mmol) and [(APTDP)(FeCl<sub>4</sub>)<sub>2</sub>@HNT] (1.5 mol%, 25 mg) at 80 °C under solvent-free conditions. <sup>b</sup> Isolated yield.

**Scheme 3** [(APTDP)(FeCl<sub>4</sub>)<sub>2</sub>@HNT]-catalyzed synthesis of benzo-thiazole derivatives.**Scheme 4** [(APTDP)(FeCl<sub>4</sub>)<sub>2</sub>@HNT]-catalyzed synthesis of benzyl benzo-thiazole derivatives.

95% yields (Scheme 3). However, reactions with aliphatic nitriles, such as pentanenitrile and heptanenitrile did not give the corresponding products under the identical reaction conditions. Furthermore, 2-aminophenyl disulfide (instead of 2-aminothiophenol) did not take part in the related reactions under optimum conditions. It is also noteworthy that benzo-thiazoles were accessible on gram scales. On a 10 mmol scale, benzonitrile reacted with 2-aminothiophenol in the presence of [(APTDP)(FeCl<sub>4</sub>)<sub>2</sub>@HNT] (0.15 mol%) at 80 °C, to afford 2-phenylbenzo[d]thiazole **3a** in 70% yield after 8 h. We further examined the scope of arylacetonitriles for this reaction (Scheme 4). Interestingly, phenylacetonitrile, 4-chlorophenylacetonitrile, 4-methoxyphenylacetonitrile and 4-methylphenylacetonitrile gave desired products **5a–d** in 90–92%

**Scheme 5** Selective synthesis of mono- and bis-benzothiazoles catalyzed by [(APTDP)(FeCl<sub>4</sub>)<sub>2</sub>@HNT].

yields. Besides, diphenylacetonitrile provided the corresponding product **5e** in 92% yield.

To our delight, the  $[(\text{APTDP})(\text{FeCl}_4)_2@ \text{HNT}]$  was applied as an efficient catalyst for the selective synthesis of mono- and bis-benzothiazoles (Scheme 5). In this respect, dinitriles such as 1,3-dicyanobenzene and 1,3-phenylenediacetonitrile were used. Fortunately, the corresponding mono-benzonitrile **3o** and mono-methylphenylacetonitrile **5f** were selectively synthesized using a 1 : 1 molar ratio of starting materials, indicating that mono-products are of vital importance to provide other useful functional groups. It is also worth noting that the corresponding bis-derivatives **3p** and **5g** were selectively obtained in high yields, when a 2 : 1 molar ratio of starting materials was used (Scheme 5).

In another approach for the synthesis of tris-benzothiazole, the reaction of 2-aminothiophenol **1** (3 mmol) with 2,2',2''-(benzene-1,3,5-triyl)triacetonitrile **4h** (1 mmol) proceeded smoothly to give the corresponding symmetric tris-benzothiazole **5h** in 75% yield under solvent-free conditions (Scheme 6).

In the following, the competitive reaction of 2-aminothiophenol (1 mmol) with aromatic nitrile (4-methylbenzonitrile) (1 mmol) and aliphatic nitrile (heptanenitrile) (1 mmol) was examined under the same conditions. The results showed that 4-methylbenzonitrile was transformed to the corresponding benzothiazole **3j** in the presence of heptanenitrile. This outcome clearly indicated the selectivity performance of  $[(\text{APTDP})(\text{FeCl}_4)_2@ \text{HNT}]$  catalyst (Scheme 7).

The structure of the products was identified by their melting points, spectral data, and elemental analysis.

Although several mechanisms have been proposed for this reaction, we tried to provide the best path using density

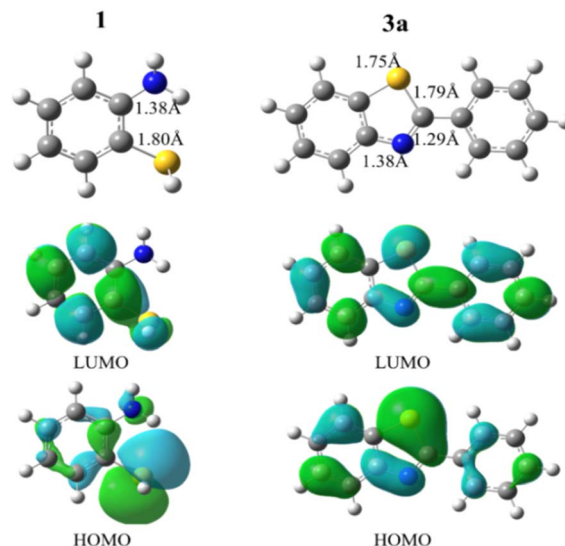
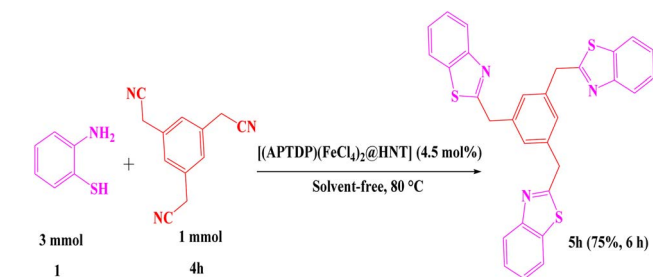


Fig. 6 Optimized geometries and spatial distributions of frontier molecular orbitals of the **1** and **3a** structures. The blue and green colors stand for electrons and holes, respectively.

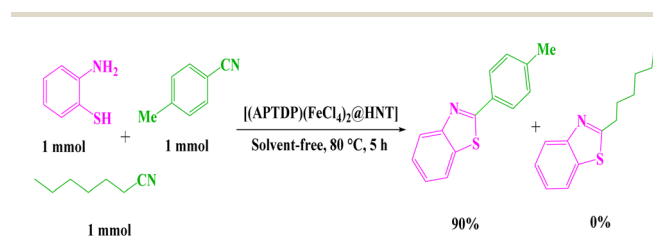
functional theory (DFT) calculations. Geometry and frequency calculations were carried out using B3LYP<sup>19</sup> functional implemented in Gaussian 09.<sup>20</sup> The van der Waals (vdW) interaction is performed by the semiempirical long-range DFT-D3 method.<sup>21</sup> All configurations were fully optimized with default convergence criteria. Besides, frequency calculations were performed to ensure that there are no imaginary frequencies for minima. First, we investigated the electronic properties of 2-aminothiophenol (structure **1**) and benzothiazole derivative (structure **3a**). Fig. 6 represents the most stable geometries of the **1** and **3a** structures together with bond length parameters.

The results show that the **3a** has a longer C–N bond with 1.38 Å and a smaller C–N bond with a distance of 1.29 Å. Also, the C–S bond lengths in the **1** and **3a** structures are about 1.80 Å and 1.75 Å, respectively. The natural bond orbital (NBO) analysis reveals that the nitrogen atoms carry the negative charge of respectively, 0.79e and 0.51e in the **1** and **3a** structures. Also, the results show a negative charge of 0.09e and a positive charge of 0.21e for the S atoms in the **1** and **3a** structures, respectively. As frontier molecular orbital analysis shows, the HOMOs of the **1** and **3a** structures are mostly localized on the S and N atoms, while the LUMOs are approximately distributed along the whole molecular framework (Fig. 6). The calculated HOMO–LUMO energy gaps for the **1** and **3a** structures are 5.24 eV and 4.46 eV, respectively. In order to explore the favorable mechanisms, we have examined two possible mechanisms for the model reaction between  $[(\text{APTDP})(\text{FeCl}_4)_2@ \text{HNT}]$  and benzonitrile (Scheme 8).

The use of  $(\text{APTDP})(\text{FeCl}_4)_2$  instead of  $[(\text{APTDP})(\text{FeCl}_4)_2@ \text{HNT}]$  was due to its lower steric factor which is more appropriate for theoretical studies. Table 2 gathered the Gibbs reaction energies of the two mechanisms, and the corresponding free energy profiles are represented in Fig. 7. Moreover, the geometries of the stationary points are shown in Fig. 8.



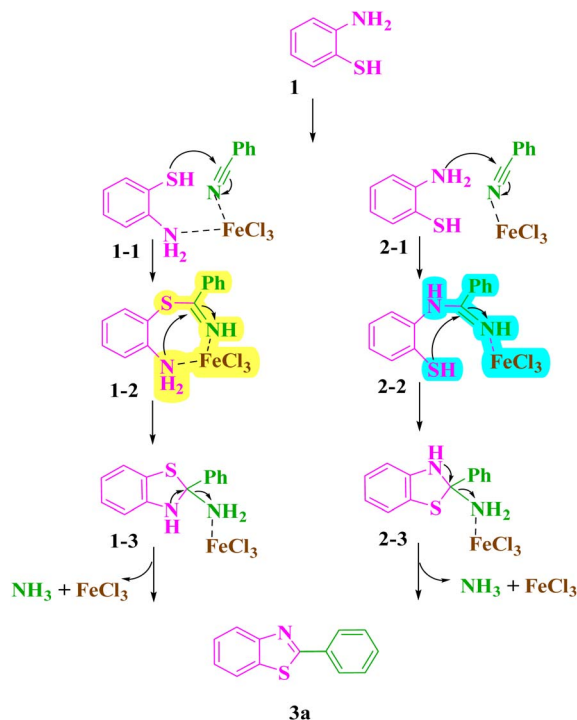
Scheme 6 Synthesis of symmetric tris-benzothiazole catalyzed by  $[(\text{APTDP})(\text{FeCl}_4)_2@ \text{HNT}]$ .



Scheme 7 Competitive reaction of 2-aminothiophenol with 4-methylbenzonitrile and heptanenitrile in the presence of  $[(\text{APTDP})(\text{FeCl}_4)_2@ \text{HNT}]$ .







**Scheme 8** Two mechanisms (1–1 to 3a (left) and 2–1 to 3a (right)) for the synthesis of benzothiazole derivative (3a).

**Table 2** Gibbs reaction energies for the reaction between  $[(\text{APTDP})(\text{FeCl}_4)_2@ \text{HNT}]$  and benzonitrile in two proposed pathways. The calculations have been performed at 298.15 K

Mechanism 1		Mechanism 2	
$\Delta G$ (kcal mol <sup>-1</sup> )		$\Delta G$ (kcal mol <sup>-1</sup> )	
(1-1) → TS1	5.7	(2-1) → TS1	7.5
TS → (1-2)	-3.5	TS → (2-2)	-3.8
(1-2) → TS2	2.4	(2-2) → TS2	3.5
TS → (1-3)	-8.3	TS → (2-3)	-7.9
(1-3) → (3a)	-4.6	(2-3) → (3a)	-2.3

The Gibbs formation energies of the TS1 for the mechanisms 1 and 2 are, 5.7 and 7.5 kcal mol<sup>-1</sup>, respectively, that reveal a higher difference as compared to the TS2 steps. These

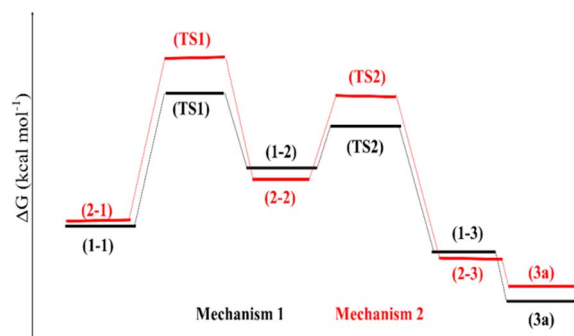


**Fig. 7** Gibbs free energy profiles for the two mechanisms.

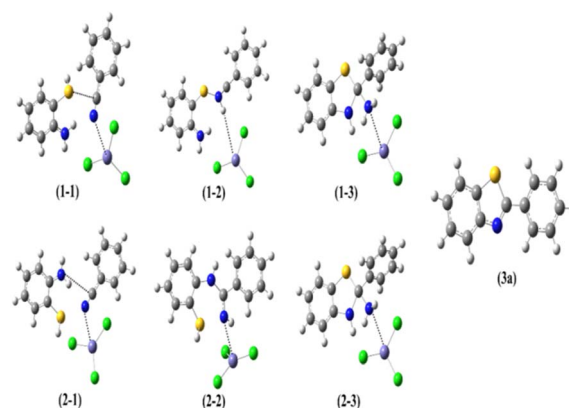
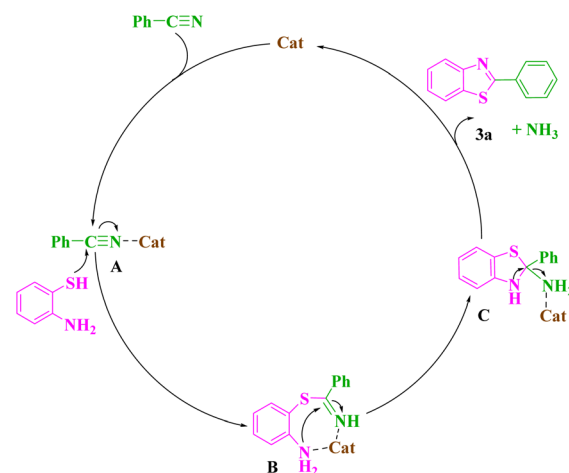


**Fig. 8** Structures of stationary points corresponding to the two proposed mechanisms in Scheme 8.

reactions involve the formation of a C–S and C–N bonds between  $[(\text{APTDP})(\text{FeCl}_4)_2@ \text{HNT}]$  and benzonitrile. Furthermore, the calculated Gibbs reaction energies for the formation of (1-3) and (2-3) complexes in the mechanisms 1 and 2 are, -8.3 kcal mol<sup>-1</sup> and -7.9 kcal mol<sup>-1</sup>, respectively. Finally, the Gibbs reaction energy for the dissociation of (1-3) to the (3a) in mechanism 1 is significantly lower than the similar step in the mechanism 2. According to these differences, the Gibbs free energy profiles for the two mechanisms predict the preference of mechanism 1 *versus* the mechanism 2. However, the differences of the Gibbs free energy values in two mechanisms are small, and due to the computational uncertainty, the mechanism 2 would be predicted to be competitive with the mechanism 1. Consequently, the most probable mechanism was proposed on the basis of theoretical study using DFT simulation method (Scheme 9). First, the benzonitrile is activated by the catalyst to give A and intermediate B by nucleophilic attack of thiol group of 2-aminothiophenol to the carbon of benzonitrile. Next, intramolecular cyclization of B in the presence of the catalyst afforded the intermediate C. Finally, elimination of  $\text{NH}_3$



**Scheme 9** Proposed reaction mechanism.

**Table 3** Comparison of the results of the synthesis of **3a** catalyzed by Zn(OAc)<sub>2</sub>, TfOH, Cu(OAc)<sub>2</sub>, Co and [(APTDP)(FeCl<sub>4</sub>)<sub>2</sub>@HNT]

Catalyst/conditions	Catalyst loading	Time (h)	Yield <sup>a</sup> (%)	TON <sup>b</sup>	TOF <sup>c</sup> (h <sup>-1</sup> )	Ref.
Zn(OAc) <sub>2</sub> · 2H <sub>2</sub> O, PMHS, 120 °C, solventless	5 mol%	18	91	18.2	1.01	15
TfOH, 100 °C	2 mol%	12	94	47.0	3.91	16
Cu(OAc) <sub>2</sub> , Et <sub>3</sub> N/EtOH, 70 °C	10 mol%	6	86	8.6	1.43	17
Co <sub>SAS</sub> -NPs/NC (0.25), 150 °C, 10 h, PhCl (2 mL)	2.5 mol%	10	92	36.8	3.68	23
[(APTDP)(FeCl <sub>4</sub> ) <sub>2</sub> @HNT]/solvent-free, 80 °C	1.5 mol%	4.5	95	63.3	14.07	This work

<sup>a</sup> Isolated yield. <sup>b</sup> Turn-over number. <sup>c</sup> Turn-over frequency.

**Table 4** Calculated green metrics (AE, CE, RME, OE and E-factor) for the synthesized compound **3a**

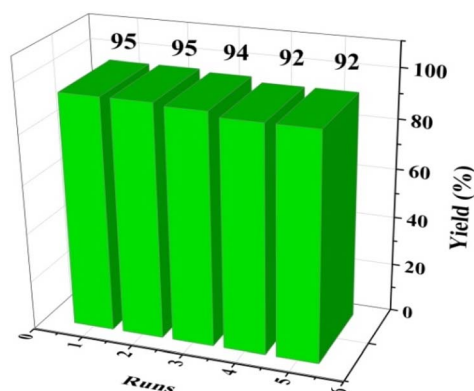
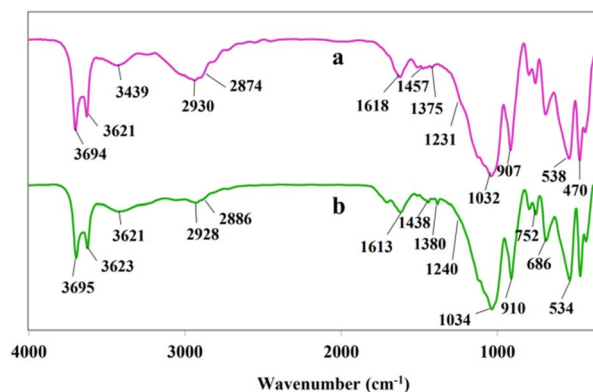
Green chemistry metrics	Ref. 15	Ref. 16	Ref. 17	This work
AE <sup>a</sup> (%)	32.99	92.57	92.57	92.57
CE <sup>b</sup> (%)	28.78	94	86	95
RME <sup>c</sup> (%)	30.05	86.85	79.82	87.72
OE <sup>d</sup> (%)	91.08	93.82	86.22	94.76
E-factor	2.32	0.15	0.25	0.14

<sup>a</sup> Atom economy. <sup>b</sup> Carbon efficiency. <sup>c</sup> Reaction mass efficiency. <sup>d</sup> Optimum efficiency.

from **C** furnishes the corresponding benzothiazole **3** and releases the catalyst for the next run.

To show the quality and reactivity of [(APTDP)(FeCl<sub>4</sub>)<sub>2</sub>@HNT], a comparison with those of some previously reported catalysts for the synthesis of **3a** is presented in Table 3. As can be seen, our catalytic system is superior to the previously documented methods in terms of catalyst loading, time, yield, TON and TOF.

Furthermore, the green chemistry metrics such as atom-economy (AE), carbon efficiency (CE), reaction mass efficiency (RME), and optimum efficiency (OE) concepts, and E-factor, have been embraced by the academic community and the chemical industry.<sup>22</sup> It is of great importance that the favourable

**Fig. 9** Reuse of [(APTDP)(FeCl<sub>4</sub>)<sub>2</sub>@HNT] examined on the model reaction.**Fig. 10** FT-IR spectra of: (a) fresh and (b) reused [(APTDP)(FeCl<sub>4</sub>)<sub>2</sub>@HNT] catalyst.

green chemistry metrics like smaller E-factor (0.14) and higher atom economy (92.57), carbon efficiency (95%), reaction mass efficiency (87.72%), and optimum efficiency (94.76%) were observed for our optimized protocol (Table 4).

The recovery and reusability of a heterogeneous catalyst is an important feature from safety and economy point of view. For this purpose, the reusability of [(APTDP)(FeCl<sub>4</sub>)<sub>2</sub>@HNT] was probed using the model reaction under the optimized conditions (Fig. 9). In this respect, the mixture was cooled to room temperature at the end of each reaction and diluted with ethyl acetate. The catalyst was separated by centrifugation, washed several times with ethyl acetate, then, dried in a vacuum oven, and finally, reused in next run. The results revealed that the catalyst could be reused for four times without noticeable change in its catalytic activity (Fig. 9). Comparison of the FT-IR spectra of fresh and recovered catalysts showed no obvious changes in the structure of the catalyst and the characteristic bands. This clearly exposed that the catalyst is stable under the reaction conditions and can be recovered and reused (Fig. 10).

## Conclusions

To summarize, a benign and facile protocol for the synthesis of benzothiazole derivatives through the reaction of 2-aminothiophenol and aryl nitriles using [(APTDP)(FeCl<sub>4</sub>)<sub>2</sub>@HNT], as a green catalyst, has been developed. The key achievement of this study is the selective synthesis of mono-, bis- and tris-





benzothiazoles from dinitrile and trinitrile in high yields and purity. Excellent yields, short reaction times, easy work-up procedure, waste-free process combined with recovery and reusability of the catalyst, mild conditions, and avoiding hazardous organic solvents are other advantages of the present method.

## Experimental section

### General

The chemicals used in this work were purchased from Fluka and Merck chemical companies. HNTs were purchased from Sigma-Aldrich (Germany) chemical company. The properties of HNTs are as follows: diameter = 30–70 nm, length = 1–3  $\mu\text{m}$ , cation exchange capacity = 8.0 meq  $\text{g}^{-1}$ , density = 2.53  $\text{g cm}^{-3}$ , average hydrodynamic diameter = 399.7 nm, specific surface area ( $a_{\text{s,BET}}$  = 39.156  $\text{m}^2 \text{g}^{-1}$ ), total pore volume = 0.214  $\text{cm}^3 \text{g}^{-1}$  and elemental compositions =  $\text{Al}_2\text{Si}_2\text{O}_5(\text{OH})_4 \cdot 2\text{H}_2\text{O}$  (1 : 1 ratio of Al/Si). Melting points were determined with a Stuart Scientific SMP2 apparatus. FT-IR spectra was recorded on a Jasco 6300 in the range of 400–4000  $\text{cm}^{-1}$ .  $^1\text{H}$  and  $^{13}\text{C}$  NMR (400 and 100 MHz) spectra were recorded on a Bruker Avance 400 MHz spectrometer using  $\text{DMSO}-d_6$  and  $\text{CDCl}_3$  as solvent. Elemental analysis was performed on a LECO, CHNS-932 analyzer. Thermogravimetric analysis (TGA) was carried out on a Mettler TG50 instrument under air flow at a uniform heating rate of 20  $^\circ\text{C min}^{-1}$  in the range 30–700  $^\circ\text{C}$ . The TGA instrument was re-calibrated at frequent intervals with standards; the accuracy was always better than  $\pm 2.0\%$ . The scanning electron microscope measurement was carried out on a Hitachi S-4700 scanning electron microscope (SEM). The transmission electron microscopy (TEM) was carried out on a Philips CM10 instrument operating at 100 kV.

### General procedure for the preparation of $[(\text{APTDP})(\text{FeCl}_4)_2@ \text{HNT}]$

**Preparation of  $[(\text{APTDP})(\text{Cl})_2@ \text{HNT}]$ .** First, the  $\text{APT}@ \text{HNT}$  was prepared according to the reported procedure.<sup>18b</sup> Intensely, the obtained  $\text{APT}@ \text{HNT}$  (2 g) and  $\text{PPh}_3$  (5.6 g) were dispersed in 40 mL dry toluene and then, the reaction mixture was refluxed for 20 hours under  $\text{N}_2$ . Lastly, the mixture was filtered and washed with toluene ( $2 \times 10 \text{ mL}$ ) and ethanol ( $2 \times 10 \text{ mL}$ ). The resulting precipitate  $[(\text{APTDP})(\text{Cl})_2@ \text{HNT}]$  dried in a vacuum oven at 80  $^\circ\text{C}$ .

**Preparation of  $[(\text{APTDP})(\text{FeCl}_4)_2@ \text{HNT}]$ .** A dispersed mixture of  $[(\text{APTDP})(\text{Cl})_2@ \text{HNT}]$  (1.65 g) and anhydrous  $\text{FeCl}_3$  (8.12 g) in dry toluene (50 mL) was refluxed for 48 hours under  $\text{N}_2$ . Next, the mixture was filtered and washed with toluene ( $3 \times 10 \text{ mL}$ ) and ethanol ( $3 \times 10 \text{ mL}$ ), respectively. Finally, the precipitate dried under vacuum for 2 hours at 80  $^\circ\text{C}$  to afford the  $[(\text{APTDP})(\text{FeCl}_4)_2@ \text{HNT}]$  nanocatalyst (Scheme 2).

**General procedure for synthesis of mono-benzothiazole derivatives catalyzed by  $[(\text{APTDP})(\text{FeCl}_4)_2@ \text{HNT}]$ .** A mixture of 2-aminothiophenol (1.0 mmol), nitrile derivative (1.0 mmol) and  $[(\text{APTDP})(\text{FeCl}_4)_2@ \text{HNT}]$  (1.5 mol%, 25 mg) was stirred at 80  $^\circ\text{C}$  under solvent-free conditions for suitable time according to Schemes 3 and 4. After completion of the reaction as shown

by TLC (eluent : petroleum ether/ethyl acetate, 5 : 1), the mixture was cooled to room temperature and ethyl acetate (5 mL) was added. Then, the catalyst was separated by centrifugation and washed with ethyl acetate ( $3 \times 5 \text{ mL}$ ). The organic residue was purified by column chromatography on silica gel (petroleum ether/ethyl acetate) to give the pure product in 90–96% yields (Scheme 3, 3a–n and Scheme 4, 5a–e).

**Synthesis of bis-benzothiazole derivatives catalyzed by  $[(\text{APTDP})(\text{FeCl}_4)_2@ \text{HNT}]$ .** 2-Aminothiophenol (2.0 mmol), 1,3-dicyanobenzene and/or 1,3-phenylenediacetonitrile (1.0 mmol) and  $[(\text{APTDP})(\text{FeCl}_4)_2@ \text{HNT}]$  (3 mol%, 50 mg) was stirred at 80  $^\circ\text{C}$  under solvent-free conditions for the duration of appropriate time mentioned in Scheme 5. The progress of the reaction was monitored by TLC (eluent : petroleum ether/ethyl acetate, 5 : 1). Upon completion, the work-up was done as defined for synthesis of mono-benzothiazoles and the desired products were obtained in 78–80% yields (Scheme 5, 3p and 5g).

**Synthesis of tris-benzothiazole derivative catalyzed by  $[(\text{APTDP})(\text{FeCl}_4)_2@ \text{HNT}]$ .** 2-Aminothiophenol (3.0 mmol), 2,2',2''-(benzene-1,3,5-triyl)triacetoneitrile (1.0 mmol) and  $[(\text{APTDP})(\text{FeCl}_4)_2@ \text{HNT}]$  (4.5 mol%, 75 mg) was stirred at 80  $^\circ\text{C}$  under solvent-free conditions for 6 hours. On completion of the reaction, as evident from the TLC analysis (eluent : petroleum ether/ethyl acetate, 5 : 1), the work-up was carried out as described for synthesis of mono-benzothiazoles and the corresponding product was gained in 75% isolated yield (Scheme 6, 5h).

## Abbreviations

HNTs	Halloysite nanotubes
ILs	Ionic liquids
APTS	(3-Aminopropyl)triethoxysilane
TCT	1,3,5-Trichlorotriazine
DIPEA	<i>N,N</i> -Diisopropylethylamine
THF	Tetrahydrofuran
$\text{PPh}_3$	Triphenylphosphine
<i>p</i> -TSA	<i>p</i> -Toluenesulfonic acid
TLC	Thin layer chromatography

## Conflicts of interest

There are no conflicts to declare.

## Acknowledgements

The authors are grateful to the Research Council of the University of Isfahan for financial support of this work.

## Notes and references

- (a) C. S. Buettner, A. Cognigni, C. Schröder and K. Bica-Schröder, *J. Mol. Liq.*, 2022, **347**, 118160–118191; (b) V. S. Sivasankarapillai, A. Sundararajan, E. C. Easwaran, M. Pourmadadi, A. Aslani, R. Dhanusuraman, A. Rahdar and G. Z. Kyzas, *J. Mol. Liq.*, 2023, **382**, 121846–121856; (c)



- R. Goutham, P. Rohit, S. S. Vigneshwar, A. Swetha, J. Arun, K. P. Gopinath and A. Pugazhendhi, *J. Mol. Liq.*, 2022, **349**, 118150–118160; (d) K. Dong, X. Liu, V. Dong, X. Zhang and S. Zhang, *Chem. Rev.*, 2017, **117**, 6636–6695; (e) C. Dai, J. Zhang, C. Huang and Z. Lei, *Chem. Rev.*, 2017, **117**, 6929–6983; (f) B. Wang, L. Qin, T. Mu, Z. Xue and G. Gao, *Chem. Rev.*, 2017, **117**, 7113–7131.
- 2 (a) S. T. Hemp, M. Zhang, M. H. Allen Jr., S. Cheng, R. B. Moore and T. E. Long, *Macromol. Chem. Phys.*, 2013, **214**, 2099–2107; (b) K. Tsunashima, E. Niwa, S. Kodama, M. Sugiya and Y. Ono, *J. Phys. Chem. B*, 2009, **113**, 15870–15874; (c) K. Tsunashima, S. Kodama, M. Sugiya and Y. Kunugi, *Electrochim. Acta*, 2010, **56**, 762–766; (d) K. Tsunashima, A. Kawabata, M. Matsumiya, S. Kodama, R. Enomoto, M. Sugiya and Y. Kunugi, *Electrochem. Commun.*, 2011, **13**, 178–181; (e) J. Luo, O. Conrad and I. F. Vankelecom, *J. Mater. Chem.*, 2012, **22**, 20574–20579; (f) U. A. Rana, R. Vijayaraghavan, M. Walther, J. Sun, A. A. Torriero, M. Forsyth and D. R. MacFarlane, *Chem. Commun.*, 2011, **47**, 11612–11614; (g) A. C. Barsanti, C. Chiappe, T. Ghilardi and C. S. Pomelli, *RSC Adv.*, 2014, **4**, 38848–38854.
- 3 (a) M. J. Saif, H. M. Asif and M. Naveed, *J. Chil. Chem. Soc.*, 2018, **63**, 4109–4125; (b) X. Ding, H. Wang, W. Chen, J. Liu and Y. Zhang, *RSC Adv.*, 2014, **4**, 41993–41996; (c) L. Duan, W. Huang and Y. Zhang, *RSC Adv.*, 2015, **5**, 6666–6674; (d) Z. Hajizadeh and A. Maleki, *Mol. Catal.*, 2018, **460**, 87–93.
- 4 (a) N. Bálamo, S. Mendieta, A. Heredia and M. Crivello, *Mol. Catal.*, 2020, **481**, 110290–110299; (b) V. Bertolino, G. Cavallaro, G. Lazzara, S. Milioto and F. Parisi, *Langmuir*, 2017, **33**, 3317–3323; (c) S. Sadjadi, M. M. Heravi, M. Malmir and B. Masoumi, *Appl. Organomet. Chem.*, 2018, **32**, 4113–4125; (d) S. Sadjadi, M. M. Heravi, M. Malmir and F. G. Kahangi, *Appl. Clay Sci.*, 2018, **162**, 192–203; (e) S. Sadjadi, M. Malmir and M. M. Heravi, *Appl. Clay Sci.*, 2019, **168**, 184–195; (f) S. Sadjadi, G. Lazzara, M. M. Heravi and G. Cavallaro, *Appl. Clay Sci.*, 2019, **182**, 105299–105313; (g) B. Eftekhari far and M. Nasr-Esfahani, *Appl. Organomet. Chem.*, 2020, **34**, 5406–5419.
- 5 (a) X. Ding, H. Wang, W. Chen, J. Liu and Y. Zhang, *RSC Adv.*, 2014, **4**, 41993–41996; (b) L. Yu, Y. Zhang, B. Zhang and J. Liu, *Sci. Rep.*, 2014, **4**, 4551–4556; (c) J. Kurczewska, M. Cegłowski, B. Messyas and G. Schroeder, *Appl. Clay Sci.*, 2018, **153**, 134–143; (d) Z. Long, Y. P. Wu, H. Y. Gao, Y. F. Li, R. R. He and M. Liu, *Bioconjugate Chem.*, 2018, **29**, 2606–2618; (e) S. Ramanayaka, B. Sarkar, A. T. Cooray, Y. S. Ok and M. Vithanage, *J. Hazard. Mater.*, 2020, **384**, 121301–121327.
- 6 S. M. Stagnaro, C. Volzone and L. Huck, *Procedia Mater. Sci.*, 2015, **8**, 586–591.
- 7 (a) R. K. Deshmukh, L. Kumar and K. K. Gaikwad, *Appl. Clay Sci.*, 2023, **234**, 106856–106866; (b) D. Cheikh, H. Majdoub and M. Darder, *Appl. Clay Sci.*, 2022, **216**, 106335–106345.
- 8 (a) J. Nishiu, M. Ito, Y. Ishida, M. Kakutani, T. Shibata, M. Matsushita and M. Shindo, *Diabetes, Obes. Metab.*, 2006, **8**, 508–516; (b) L. Leventhal, M. R. Brandt, T. A. Cummons, M. J. Piesla, K. E. Rogers and H. A. Harris, *Eur. J. Pharmacol.*, 2006, **553**, 146–148; (c) W. S. Saari, J. M. Hoffman, J. S. Wai, T. E. Fisher, C. S. Rooney, A. M. Smith, C. M. Thomas, M. E. Goldman and J. A. O'Brien, *J. Med. Chem.*, 1991, **34**, 2922–2925; (d) L. Q. Sun, J. Chen, K. Takaki, G. Johnson, L. Iben, C. D. Mahle, E. Ryan and C. Xu, *Bioorg. Med. Chem. Lett.*, 2004, **14**, 1197–1200; (e) S. Yoshida, S. Shiokawa, K. I. Kawano, T. Ito, H. Murakami, H. Suzuki and Y. Sato, *J. Med. Chem.*, 2005, **48**, 7075–7079.
- 9 (a) M. Wang, M. Gao, B. H. Mock, K. D. Miller, G. W. Sledge, G. D. Hutchins and Q. H. Zheng, *Bioorg. Med. Chem.*, 2006, **14**, 8599–8607; (b) R. Bazzi, T. D. Bradshaw, J. C. Rowlands, M. F. Stevens and D. R. Bell, *Toxicol. Appl. Pharmacol.*, 2009, **237**, 102–110; (c) K. Wang and F. P. Guengerich, *Chem. Res. Toxicol.*, 2012, **25**, 1740–1751.
- 10 (a) C. G. Mortimer, G. Wells, J. P. Crochard, E. L. Stone, T. D. Bradshaw, M. F. Stevens and A. D. Westwell, *J. Med. Chem.*, 2006, **49**, 179–185; (b) S. Aiello, G. Wells, E. L. Stone, H. Kadri, R. Bazzi, D. R. Bell, M. F. Stevens, C. S. Matthews, T. D. Bradshaw and A. D. Westwell, *J. Med. Chem.*, 2008, **51**, 5135–5139.
- 11 B. L. Mylari, E. R. Larson, T. A. Beyer, W. J. Zembrowski, C. E. Aldinger, M. F. Dee, T. W. Siegel and D. H. Singleton, *J. Med. Chem.*, 1991, **34**, 108–122.
- 12 (a) M. A. Butters, W. E. Klunk, C. A. Mathis, J. C. Price, S. K. Ziolko, J. A. Hoge, N. D. Tsopelas, B. J. Lopresti, C. F. Reynolds III, S. T. DeKosky and C. C. Meltzer, *Alzheimer Dis. Assoc. Disord.*, 2008, **22**, 261–268; (b) W. E. Klunk, B. J. Lopresti, M. D. Ikonovic, I. M. Lefterov, R. P. Koldamova, E. E. Abrahamson, M. L. Debnath, D. P. Holt, G. F. Huang, L. Shao and S. T. DeKosky, *J. Neurosci.*, 2005, **25**, 10598–10606; (c) B. J. Lopresti, W. E. Klunk, C. A. Mathis, J. A. Hoge, S. K. Ziolko, X. Lu, C. C. Meltzer, K. Schimmel, N. D. Tsopelas, S. T. DeKosky and J. C. Price, *J. Nucl. Med.*, 2005, **46**, 1959–1972.
- 13 K. D. Dhawale, A. P. Ingale, S. V. Shinde, N. M. Thorat and L. R. Patil, *Synth. Commun.*, 2021, **51**, 1588–1601.
- 14 I. Mohammadpoor-Baltork, A. R. Khosropour and S. F. Hojati, *Monatsh. Chem.*, 2007, **138**, 663–667.
- 15 D. B. Nale and B. M. Bhanage, *Synlett*, 2015, **26**, 2835–2842.
- 16 X. Yu, Q. Yin, Z. Zhang, T. Huang, Z. Pu and M. Bao, *Tetrahedron Lett.*, 2019, **60**, 1964–1966.
- 17 Y. Sun, H. Jiang, W. Wu, W. Zeng and X. Wu, *Org. Lett.*, 2013, **15**, 1598–1601.
- 18 (a) M. Moeini Korbekandi, I. Mohammadpoor-Baltork, M. Moghadam, S. Tangestaninejad, V. Mirkhani, A. Omidvar and B. Notash, *ACS Omega*, 2023, **8**, 15883–15895; (b) M. Samadani, B. Asadi, I. Mohammadpoor-Baltork, V. Mirkhani, S. Tangestaninejad and M. Moghadam, *RSC Adv.*, 2021, **11**, 11976–11983; (c) M. Azizi, M. Nasr-Esfahani, I. Mohammadpoor-Baltork, M. Moghadam, V. Mirkhani, S. Tangestaninejad and R. Kia, *J. Org. Chem.*, 2018, **83**, 14743–14750; (d) F. Rahmani, I. Mohammadpoor-Baltork, A. R. Khosropour, M. Moghadam, S. Tangestaninejad and V. Mirkhani, *Tetrahedron Lett.*, 2016, **57**, 2294–2297; (e) F. Karimi,



- B. Tighsazzadeh, B. Asadi, I. Mohammadpoor-Baltork, M. Layeghi, V. Mirkhani, S. Tangestaninejad and M. Moghadam, *RSC Adv.*, 2022, **12**, 22180–22187; (f) B. Asadi, I. Mohammadpoor-Baltork, S. Tangestaninejad, M. Moghadam, V. Mirkhani and A. Landarani-Isfahani, *New J. Chem.*, 2016, **40**, 6171–6184; (g) B. Asadi, I. Mohammadpoor-Baltork, V. Mirkhani, S. Tangestaninejad and M. Moghadam, *ChemistrySelect*, 2020, **5**, 7840–7848; (h) T. Ataee-Kachouei, M. Nasr-Esfahani, I. Mohammadpoor-Baltork, V. Mirkhani, M. Moghadam, S. Tangestaninejad and B. Notash, *Appl. Organomet. Chem.*, 2020, **34**, 5948–5965.
- 19 A. D. Becke, *J. Chem. Phys.*, 1993, **98**, 5648–5652.
- 20 M. J. Frisch, G. W. Trucks, H. B. Schlegel, G. E. Scuseria, M. A. Robb, J. R. Cheeseman, G. Scalmani, V. Barone, B. Mennucci, G. A. Petersson and H. Nakatsuji, Gaussian Inc., Wallingford CT, 2009, p. 139.
- 21 S. J. Grimme, *Comput. Chem.*, 2006, **27**, 1787–1799.
- 22 (a) F. I. McGonagle, H. F. Sneddon, C. Jamieson and A. J. Watson, *ACS Sustainable Chem. Eng.*, 2014, **2**, 523–532; (b) A. D. Curzons, D. J. Constable, D. N. Mortimer and V. L. Cunningham, *Green Chem.*, 2001, **3**, 1–6.
- 23 B. Wang, M. Li, S. Zhang, H. Wu, Y. Liao and H. Li, *Appl. Catal., B*, 2023, **327**, 122454–122469.

